Technical Reference on Hydrogen Compatibility of Materials

Austenitic Stainless Steels:
Type 316 (code 2103)

Prepared by:
C. San Marchi, Sandia National Laboratories

Editors
C. San Marchi
B.P. Somerday
Sandia National Laboratories

This report may be updated and revised periodically in response to the needs of the technical community; up-to-date versions can be requested from the editors at the address given below. The success of this reference depends upon feedback from the technical community; please forward your comments, suggestions, criticisms and relevant public-domain data to:

Sandia National Laboratories
Matls Tech Ref
C. San Marchi (MS-9402)
7011 East Ave
Livermore CA 94550.

This document was prepared with financial support from the Safety, Codes and Standards program element of the Hydrogen, Fuel Cells and Infrastructure program, Office of Energy Efficiency and Renewable Energy; Pat Davis is the manager of this program element. Sandia is a multiprogram laboratory operated by Sandia Corporation, a Lockheed Martin Company, for the United States Department of Energy under contract DE-AC04-94AL85000.

1. General

Type 316 & 316L stainless steels are metastable austenitic alloys that have molybdenum for improved corrosion resistance and high-temperature strength. Due to their high nickel and molybdenum content, this family of alloys has high stacking fault energy; a feature that promotes cross slip and is generally associated with superior hydrogen compatibility [1, 2]. Indeed, data suggest that 316 stainless steel is more resistant to hydrogen-assisted fracture than most other austenitic stainless steels and that this resistance seems to improve with nickel concentration (within the standard compositional limits).

Type 316 stainless steel is sensitive to carbide precipitation on grain boundaries between approximately 773 K and 1073 K. A low-carbon grade, designated 316L, is used to moderate this sensitization. Carbides themselves are believed to have little, if any, effect on hydrogen-assisted fracture of austenitic stainless steels [3-5]. Carbon is an austenite stabilizer and carbide precipitation in austenitic alloys has been linked to chromium depletion in adjacent areas. Regions poor in carbon and chromium are prone to strain-induced martensitic transformations and may be active hydrogen trapping sites.

The role of martensite on hydrogen embrittlement in austenitic stainless steels has not been firmly established. Although generally viewed to be neither necessary nor sufficient to explain hydrogen-assisted fracture in austenitic stainless steels, α' martensite, in both sensitized and nonsensitized microstructures, is associated with lower resistance to hydrogen embrittlement. The trend for Fe-Cr-Ni stainless steels (300-series alloys) is that higher nickel concentration suppresses the martensitic transformation temperature and thus the strain-induced martensite [6-8]. The role of high-nickel compositions in type 316 stainless steels can then be said to improve both resistance to martensitic transformations and, it appears, resistance to hydrogen-assisted fracture.

1.1 Composition

Table 1.1.1 lists the composition of several heats of 316 used to study hydrogen effects and summarized in this report. Chinese alloy HR-1 has a composition similar to nickel-rich 316 and is reported to have superior resistance to hydrogen-assisted fracture than type 316 stainless steel [9]; specifics of this alloy and its development have not been reported in the literature.

1.2 Other Designations

UNS S31600 (316), UNS S31603 (316L), UNS S31651 (316N)

2. Permeability and Solubility

Refs. [7] and [10] provide summaries of permeability and solubility data for stainless steels. Relationships for permeability and solubility fit to data for several austenitic stainless steel alloys are given in Table 2.1. Permeability can be described by a standard Arrhenius-type relationship and appears to be nearly independent of the composition and microstructure for most austenitic stainless steels [7, 10, 11]. It is important to note that permeability data are generally extrapolated from temperatures above ambient and pressures of just a few atmospheres or less. Figure 2.1 plots relationships for permeability of type 316 stainless steels from a number of studies.

Solubility data are normally determined from the ratio of permeability and diffusivity. As a consequence of the large uncertainty typically associated with these data, in particular diffusivity, solubility data from the literature commonly vary by an order of magnitude, as shown in Figure 2.2. Ref. [10] shows that nitrogen additions to type 316 stainless steel (type 316N) do not significantly affect hydrogen solubility at low hydrogen pressures. In addition, careful comparison of diffusivity data suggests that, unlike permeability, diffusivity varies with alloy composition and/or microstructure [10], implying that solubility will also vary with alloy composition and/or microstructure. This is supported by hydrogen analysis of a number of stainless steels that have been thermally precharged with hydrogen and it isotopes, showing that hydrogen concentrations can be alloy dependent [6, 12, 13].

3. Mechanical Properties: Effects of Gaseous Hydrogen

3.1 Tensile properties

3.1.1 Smooth tensile properties

Room temperature tensile properties of 316 in gaseous hydrogen generally show little or no loss in ductility, Table 3.1.1.1. An important exception to this trend reported significant loss in ductility for high-energy rate forged material that had been thermally precharged in gaseous hydrogen and tested in high-pressure hydrogen gas, Figure 3.1.1.1; the absolute ductility determined in that study, however, remained relatively high (RA ≥ 50%), while the strength of the material was not reported. Ductility loss of about 10% (reduction of area in hydrogen relative to reduction of area in helium, RRA ~ 0.9) was noted in a low nickel 316 alloy (heat H98) when tested in 1 MPa gaseous hydrogen at room temperature [5]. Strain-induced α' martensite was observed to be distributed throughout the grains in that study.

Ductility loss was also reported for material that was thermally precharged, Table 3.1.1.1, however, the thermal precharging cycle was in the sensitization range of this alloy [14]. The nickel content of this heat (R84, Table 1.1.1) is at the lower limit of the UNS designation, and strain-induced martensite was observed. These data also differ in that the material was tested as thin sheet specimens, which are thought to be more sensitive to surface flaws than standard bar specimens [15]. Effects of hydrogen on the flow stress of type 316 stainless steel are discussed in detail in Refs. [14, 16].

Low temperature has been shown to have a significant effect on the hydrogen-assisted fracture of type 316 stainless steel. Smooth bar tensile properties of 316 at several temperatures between 380 K and 200 K, Table 3.1.1.2, show relatively modest changes in strength and ductility due to thermal precharging with hydrogen [8]. Testing in 1 MPa hydrogen gas, however, shows a significant reduction in ductility (as measured by the ratio of reduction in area in hydrogen to helium) at 150 and 220 K, but essentially no ductility loss at 80K [5]. Both sets of data show the greatest ductility loss due to hydrogen near 200 K, Figure 3.1.1.2. In addition to the difference in hydrogen source (internal versus external) in these two studies, the nickel content is substantially different in the two tested alloys. The lower nickel content of heat H98 may explain the greater susceptibility to hydrogen. This view must be expressed with caution, however, since the relative yield strengths of these alloys is not known, nor is the data sufficient to address differences between testing in the presence of internal or external hydrogen.

Tensile properties at elevated temperatures show no effect of internal hydrogen (thermal precharging) except for a slight decrease in reduction of area for temperatures from ambient to ~900 K and modest solute hardening near 600 K, Figures 3.1.1.3 and 3.1.1.4. Test specimens were heated to the test temperature rapidly (about one minute) and tests were performed at rapid extension rates (0.21 mm/s) to reduce loss of hydrogen during heating and testing [17].

3.1.2. Notched tensile properties
Notched tensile specimens show no difference in properties when tested in 69 MPa helium or hydrogen, Table 3.1.2.1.

3.2 Fracture mechanics

3.2.1 Fracture toughness
J-integral fracture toughness of high-energy rate forgings (HERF) has been reported to strongly depend on the orientation of the microstructure and to be significantly reduced when thermally precharged with deuterium and tested in hydrogen gas [18]. Due to the difficulty of instrumenting fracture specimens in high-pressure hydrogen gas, the J_m and tearing modulus (dJ/da) at maximum load are used in that study for comparison of orientations and testing conditions (values at maximum load do not represent a standardized fracture toughness). In addition, the alloy used in that study had a high volume of inclusions, which is believed to have biased the results to lower values [18]. Nonetheless, it was observed that in most cases thermally precharging the material (69 MPa hydrogen at 520 K for 7 days) was necessary to produce an effect of hydrogen on both the fracture toughness and the tearing modulus.

Ref. [19] shows that both sensitization (see section 4.2) and cathodic charging with hydrogen lowered fracture toughness.

3.2.2 Threshold stress intensity
Low-strength austenitic microstructures (<700 MPa) have been shown to have high resistance to cracking in high-pressure hydrogen gas environments under static loads [20]. Data for 316 in two microstructural conditions are given in Table 3.2.2.1.

3.3 Fatigue
No known published data in hydrogen gas.

3.4 Creep
No known published data in hydrogen gas.

3.5 Impact
No known published data in hydrogen gas.

3.6 Disk rupture testing

Disk rupture tests indicate that type 316 stainless steel with low carbon and high nickel (heat A87, designated 316ELC) is not susceptible to high-pressure hydrogen gas in the annealed condition or the 60% cold worked condition [21]. In comparison, type 316 alloys with lower nickel and higher carbon displayed a slightly lower rupture pressure in hydrogen than helium [21]. At low temperatures (~220 K) the rupture pressure of 316L was reduced about 30% in hydrogen compared to helium and martensitic phases were detected [22]. Welded disks of 316L stainless steel were also reported to be more susceptible to rupture in hydrogen at room temperature and lower temperatures as compared to the base metal [22], see also section 4.3.

4. Metallurgical considerations

4.1 Primary processing

Electroslag remelting (ESR) of type 316 stainless steel improved the fracture toughness of cathodically charged material to values greater than determined for unrefined, annealed 316 of nominally the same composition [19]. Higher annealing temperatures were also found in this study to improve the fracture toughness of charged and sensitized materials.

4.2 Heat treatment

Type 316 stainless steel shows a larger susceptibility to hydrogen embrittlement (1 MPa gaseous H_2) in smooth tensile bars when sensitized (973 K for 24 h) compared to solution-annealed microstructures, Figure 3.1.1.2 [5]. Solution-annealed microstructures (of both type 304 and 316 stainless steels) featured strain-induced α' martensite distributed through the grain structure and transgranular fracture, while sensitized microstructures featured α' martensite preferentially along grain boundaries and intergranular failure [5]. The transition from transgranular failure to intergranular fracture is accompanied by loss in ductility. There is no direct evidence that the martensite contributes to fracture, however, it is speculated that α' martensite may facilitate hydrogen accumulation at the crack tip by enhancing hydrogen mobility [5], or perhaps by acting as trapping sites for hydrogen.

In another study, high-pressure hydrogen gas (70 MPa) did not affect the ductility of 316 stainless steel heat treated for 2 hours at 1323 K [23]. Both smooth (Table 4.2.1) and notched (Table 4.2.2) tensile geometries were tested. This temperature is greater than typically associated with sensitization of stainless steels, which may explain the absence of a sensitization effect. The composition of this alloy is not known, but the general lack of susceptibility observed in this study for 316 base metal and welds is shared with 316 alloys that have nickel compositions toward the higher end of the nickel specification for 316 alloys.

4.3 Properties of welds

Electron beam (EB) and gas tungsten arc (GTA) welds were found to be unaffected by high-pressure hydrogen gas in tension [23]. Flat-plate tensile specimens were tested in both smooth (Table 4.3.1) and notched (Table 4.3.2) geometries. Segregated microstructures were observed in the welds, and the fracture surfaces displayed ductile-dimple failure.

Welded disks of type 316L stainless steel containing 8.5% ferrite ruptured at 15-20% lower pressures in hydrogen than helium in disk rupture tests [22]. The welded and base metal disks performed equally well in helium.

Laser Engineered Net Shaping (LENS™) is a process that has features analogous to fusion welding processes: powders are melted with a laser, solidified on a substrate and built-up in subsequent passes. The ductility of smooth tensile bars machined from LENS™-fabricated 316 materials has been reported in Ref. [24]. The loss of ductility due to thermal precharging with hydrogen (138 MPa gaseous hydrogen at 300˚C for 10 days) was found to be greater in LENS™ compared to a wrought 316 [24] and to data from Table 3.1.1.2. Fracture was localized near interlayer boundaries in hydrogen precharged specimens with secondary cracking near interpass boundaries normal to the fracture surface.

5. References

1. MR Louthan, GR Caskey, JA Donovan and DE Rawl. Hydrogen Embrittlement of Metals. Mater Sci Eng 10 (1972) 357-368.
2. BC Odegard, JA Brooks and AJ West. The Effect of Hydrogen on Mechanical Behavior of Nitrogen-Strengthened Stainless Steel. in: AW Thompson and IM Bernstein, editors. Effect of Hydrogen on Behavior of Materials. New York: TMS (1976) p. 116-125.
3. AW Thompson. The Behavior of Sensitized 309S Stainless Steel in Hydrogen. Mater Sci Eng 14 (1974) 253-264.
4. CL Briant. Hydrogen Assisted Cracking of Sensitized 304 Stainless Steel. Metall Trans 9A (1978) 731-733.
5. G Han, J He, S Fukuyama and K Yokogawa. Effect of strain-induced martensite on hydrogen environment embrittlement of sensitized austenitic stainless steels at low temperatures. Acta mater 46 (1998) 4559-4570.
6. GR Caskey. Hydrogen Damage in Stainless Steel. in: MR Louthan, RP McNitt and RD Sisson, editors. Environmental Degradation of Engineering Materials in Hydrogen. Blacksburg VA: Laboratory for the Study of Environmental Degradation of Engineering Materials, Virginia Polytechnic Institute (1981) p. 283-302.
7. GR Caskey. Hydrogen Effects in Stainless Steels. in: RA Oriani, JP Hirth and M Smialowski, editors. Hydrogen Degradation of Ferrous Alloys. Park Ridge NJ: Noyes Publications (1985) p. 822-862.
8. GR Caskey. Hydrogen Compatibility Handbook for Stainless Steels (DP-1643). EI du Pont Nemours, Savannah River Laboratory, Aiken SC (June 1983).
9. J Qian, J Chen, J Chen, Z Xu, W Wang and C Pan. Corrosion of austenitic stainless steel in liquid lithium. Journal of Nuclear Materials 179-181 (1991) 603-606.
10. S Xiukui, X Jian and L Yiyi. Hydrogen Permeation Behaviour in Austenitic Stainless Steels. Mater Sci Eng A114 (1989) 179-187.
11. MR Louthan and RG Derrick. Hydrogen Transport in Austenitic Stainless Steel. Corros Sci 15 (1975) 565-577.
12. GR Caskey and RD Sisson. Hydrogen Solubility in Austenitic Stainless Steels. Scr Metall 15 (1981) 1187-1190.
13. GR Caskey. Hydrogen Solution in Stainless Steels (DPST-83-425). Savannah River Laboratory, Aiken SC (May 1983).

14. Y Rosenthal, M Mark-Markowitch, A Stern and D Eliezer. Tensile Flow and Fracture Behaviour of Austenitic Stainless Steels after Thermal Aging in a Hydrogen Atmosphere. Mater Sci Eng 67 (1984) 91-107.
15. RE Stoltz. Plane Strain Tensile Testing for Measuring Environment Sensitive Fracture. Metall Trans 12A (1981) 543-545.
16. Y Rosenthal, M Mark-Markowitch, A Stern and D Eliezer. The influence of hydrogen on the plastic flow and fracture behavior of 316L stainless steel. Scr Metall 15 (1981) 861-866.
17. WC Mosley. Effects of Internal Helium on Tensile Properties of Austenitic Stainless Steels and Related Alloys at 820˚C. in: AW Thompson and NR Moody, editor. Hydrogen Effects in Materials. TMS (1996) p. 855-864.
18. MR Dietrich, GR Caskey and JA Donovan. J-Controlled Crack Growth as an Indicator of Hydrogen-Stainless Steel Compatibility. in: IM Bernstein and AW Thompson, editor. Hydrogen Effects in Metals. The Metallurgical Society of AIME (1980) p. 637-643.
19. MG Hebsur and JJ Moore. Influence of inclusions and heat treated microstructure on hydrogen assisted fracture properties of AISI 316 stainless steel. Eng Fract Mech 22 (1985) 93-100.
20. MW Perra. Sustained-Load Cracking of Austenitic Steels in Gaseous Hydrogen. in: MR Louthan, RP McNitt and RD Sisson, editors. Environmental Degradation of Engineering Materials in Hydrogen. Blacksburg VA: Laboratory for the Study of Environmental Degradation of Engineering Materials, Virginia Polytechnic Institute (1981) p. 321-333.
21. PF Azou and JP Fidelle. Very low strain rate hydrogen gas embrittlement (HGE) and fractography of high-strength, mainly austenitic stainless steels. in: MR Louthan, RP McNitt and RD Sisson, editor. Environmental Degradation of Engineering Materials III. The Pennsylvania State University, University Park PA (1987) p. 189-198.
22. J Chene, M Aucouturier, R Arnould-Laurent, P Tison and J-P Fidelle. Hydrogen Transport by Deformation and Hydrogen Embrittlement in Selected Stainless Steels. in: IM Bernstein and AW Thompson, editor. Hydrogen Effects in Metals. The Metallurgical Society of AIME (1980) p. 583-595.
23. EL Raymond and RR Vandervoort. Tensile Properties of Welded or Sensitized 316 Stainless Steel in High-Pressure Hydrogen Gas (UCRL-52128). University of California, Lawrence Livermore Laboratory, Livermore CA (Sept 1976).
24. BP Somerday, JE Smugeresky and JA Brooks. Hydrogen-assisted fracture in LENS-fabricated 316 stainless steel. in: NR Moody, AW Thompson, RE Ricker, GW Was and RH Jones, editors. Hydrogen Effects on Material Behavior and Corrosion Deformation Interactions. Warrendale PA: TMS (2003) p. 499-508.
25. ASTM. Metals and Alloys in the UNIFIED NUMBERING SYSTEM (SAE HS-1086 OCT01; ASTM DS-56H). Society of Automotive Engineers; American Society for Testing and Materials, (2001).
26. RJ Walter and WT Chandler. Effects of High-Pressure Hydrogen on Metals at Ambient Temperature: Final Report (NASA CR-102425). Rocketdyne (report no. R-7780-1) for the National Aeronautics and Space Administration, Canoga Park CA (February 1969).
27. TL Capeletti and MR Louthan. The Tensile Ductility of Austenitic Steels in Air and Hydrogen. J Eng Mater Technol 99 (1977) 153-158.
28. RP Jewitt, RJ Walter, WT Chandler and RP Frohmberg. Hydrogen Environment Embrittlement of Metals (NASA CR-2163). Rocketdyne for the National Aeronautics and Space Administration, Canoga Park CA (March 1973).

29. RE Stoltz, NR Moody and MW Perra. Microfracture Model for Hydrogen Embrittlement of Austenitic Steels. Metall Trans 14A (1983) 1528-1531.
30. AI Gromov and YK Kovneristyi. Permeability, Diffusion, and Solubility of Hydrogen in Cr-Ni and Cr-Mn Austenitic Steels. Met Sci Heat Treat 22 (1980) 321-324.
31. EHV Deventer and VA Maroni. Hydrogen Permeation Characteristics of some Austenitic and Nickel-base Alloys. J Nucl Mater 92 (1980) 103-111.
32. T Tanabe, Y Tamanishi, K Sawada and S Imoto. Hydrogen Transport in Stainless Steels. J Nucl Mater 122&123 (1984) 1568-1572.
33. E Hashimoto and T Kino. Hydrogen Permeation Through Type 316 Stainless Steels and Ferritic Steel for Fusion Reactor. J Nucl Mater 133&134 (1985) 289-291.
34. KS Forcey, DK Ross, JCB Simpson and DS Evans. Hydrogen Transport and Solubility in 316L and 1.4914 Steels for Fusion Reactor Applications. J Nucl Mater 160 (1988) 117-124.
35. DM Grant, DL Cummings and DA Blackburn. Hydrogen in 316 Steel - Diffusion, Permeation and Surface Reaction. J Nucl Mater 152 (1988) 139-145.
36. T Shiraishi, M Nishikawa, T Tamaguchi and K Kenmotsu. Permeation of mulit-component hydrogen isotopes through austenitc stainless steels. J Nucl Mater 273 (1999) 60-65.
37. AJ West and MR Louthan. Dislocation Transport and Hydrogen Embrittlement. Metall Trans 10A (1979) 1675-1682.

Table 1.1.1. Composition of several heats of 316 stainless steel used to study hydrogen effects as well as limits specified by the Unified Numbering System for 316 (UNS 31600) and 316L (UNS 31603).

Heat	Fe	Cr	Ni	Mn	Mo	Si	C	other	Ref.
UNS 31600	Bal	16.00 18.00	10.00 14.00	2.00 max	2.00 3.00	1.00 max	0.08 max	0.030 max S; 0.045 max P	[25]
UNS 31603	Bal	16.00 18.00	10.00 14.00	2.00 max	2.00 3.00	1.00 max	0.03 max	0.030 max S; 0.045 max P	[25]
W69	Bal	17.52	12.45	1.73	2.67	0.56	0.05	0.024 P; 0.022 S; 0.22 Cu	[26]
O76	Bal	17.41	13.51	1.56	2.53	0.71	0.061		[2]
P81	Bal	17.5	13.5	0.06	2.5	0.17	0.05	0.07 N	[20]
R84	Bal	17.7	10.2	1.4	1.6	0.6	0.029	Designated 316L	[14]
A87	Bal	16.9	13.9	1.42	2.5	0.38	0.008	0.003 S; 0.0114 P	[21]
H98	Bal	17.10	10.05	0.66	2.02	0.48	0.040	0.002 S; 0.010 P	[5]

Table 2.1. Permeability and solubility data, averages determined for several austenitic stainless steels. Permeability from Ref. [11] is determined for deuterium and has been corrected here to give permeability of hydrogen by multiplying by the square root of the mass ratio: $\sqrt{2}$. Solubility is assumed to be independent of isotope.

Temperature Range (K)	Pressure Range (MPa)	$\Phi = \Phi_o \exp(-E_\Phi / RT)$		$S = S_o \exp(-E_S / RT)$		Ref.
		Φ_o (mol m^{-1} s^{-1} MPa$^{-1/2}$)	E_Φ (kJ/mol)	S_o (mol m^{-3} MPa$^{-1/2}$)	E_S (kJ/mol)	
423-700	0.1-0.3	1.2 x 10^{-4}	59.8	179	5.9	[11]
473-703	0.1	2.81 x 10^{-4}	62.27	488	8.65	[10]

Table 3.1.1.1. Tensile properties of 316 stainless steel tested at room temperature in air, in high-pressure gaseous environments (hydrogen or helium), or thermally precharged in gaseous hydrogen and tested in air.

Material	Thermal precharging	Test environment	Strain rate (s^{-1})	S_y (MPa)	S_u (MPa)	El_u (%)	El_t (%)	RA (%)	Ref.
Not specified	None	69 MPa He	---	214	496	---	68	78	[1, 27]
	None	69 MPa H_2		214	524	---	72	77	
Cold drawn rod, heat W69	None	69 MPa He	0.67 $\times10^{-3}$	441	648	---	59	72	[26, 28]
	None	69 MPa H_2		---	683	---	56	75	
Annealed plate, heat O76	None	Air	3 $\times10^{-3}$	262	579	---	68	78	[2]
	None	69 MPa H_2		221	524	---	72	77	
Annealed sheet	None	Air	0.6 $\times10^{-3}$	263	568	---	90	75	[23]
	None	70 MPa He		248	565	---	85	70	
	None	70 MPa H_2		249	566	---	85	75	
Sensitized thin sheet, heat R84	(1) – Ar	Air	0.5 $\times10^{-3}$	327*	685	62	63	---	[14]
	(1) – H_2	Air		331*	691	43	51	---	

* stress at 0.2% strain

(1) 0.5 MPa hydrogen or argon gas, 873K, 170 hours: measured concentration of ~6 wppm hydrogen (300-325 appm)

Table 3.1.1.2. Effect of internal hydrogen (thermal precharging in high-pressure hydrogen gas) on tensile properties of 316 at low temperatures tested in air, from Ref. [8]; composition and metallurgical condition not given.

Test temperature (K)	Thermal precharging	Flow stress* (MPa)	Ultimate Stress† (MPa)	El_u (%)	El_t (%)	RA (%)
380	None	810	830	7	20	80
	(1)	880	930	11	22	70
273	None	890	1040	21	33	77
	(1)	990	1160	20	32	68
250	None	900	1150	27	40	78
	(1)	1030	1280	24	35	66
200	None	960	1210	24	43	79
	(1)	1100	1410	26	37	65

* true stress at 5% strain

† true stress at maximum load

(1) 69 MPa hydrogen gas, 620 K, 3 weeks

Table 3.1.2.1. Notched tensile properties of type 316 stainless steel tested at room temperature in air and high-pressure hydrogen and helium gas.

Material	Specimen	Thermal precharging	Test environment	Displacement rate (mm/s)	S_y (MPa)	σ_s (MPa)	RA (%)	Ref.
Cold drawn rod, heat W69	(1)	None	69 MPa He	0.4×10^{-3}	441†	1110	18	[26, 28]
		None	69 MPa H_2		---	1110	19	
Annealed sheet	(2)	None	Air	8.3×10^{-3}	345	625	70	[23]
		None	70 MPa He		298	608	80	
		None	70 MPa H_2		331	618	70	

† yield strength of smooth tensile bar
(1) V-notched specimen: 60˚ included angle; minimum diameter = 3.81 mm (0.15 inch); maximum diameter = 7.77 mm (0.306 inch); notch root radius = 0.024 mm (0.00095 inch). Stress concentration factor (K_t) = 8.4.
(2) Dog-bone notched specimens. Gage: length = 13 mm; width = 5 mm; thickness = 2.3 mm. V-notch: 60˚ included angle; depth = 0.6 mm; maximum root radius = 0.05 mm.

Table 3.2.2.1. Threshold stress intensity for type 316 stainless steel in high-pressure hydrogen gas from Ref. [20], heat P81 (data also reported in Ref. [29]).

Condition	S_y (MPa)	RA (%)	Threshold Stress Intensity (MPa $m^{1/2}$)	
			100 MPa H_2	200 MPa H_2
HERF 840˚C, WQ	689	65	NCP 132	NCP 132
WR 600˚C, WQ	903	70	---	99†

HERF = high-energy rate forging, WQ = water quench, WR = warm roll
NCP = no crack propagation at given stress intensity
† did not satisfy plane strain requirements for analysis of stress intensity

Table 4.2.1. Tensile properties of "sensitized" type 316 stainless steel tested at room temperature in air and high-pressure hydrogen and helium gas.

Material	Thermal precharging	Test environment	Strain rate (s^{-1})	S_y (MPa)	S_u (MPa)	El_u (%)	El_t (%)	RA (%)	Ref.
Rolled rod; HT 1323K, 2h, WQ	None	Air	0.6 x10^{-3}	232	558	---	78	80	[23]
	None	70 MPa He		250	658	---	68	80	
	None	70 MPa H_2		230	667	---	65	75	
Rolled rod: HT 1323K, 2h, AC	None	Air	0.6 x10^{-3}	213	558	---	76	80	[23]
	None	70 MPa He		218	639	---	68	75	
	None	70 MPa H_2		248	642	---	70	75	
Rolled rod: HT 1323K, 2h, FC	None	Air	0.6 x10^{-3}	212	561	---	75	80	[23]
	None	70 MPa He		222	666	---	72	80	
	None	70 MPa H_2		240	671	---	68	80	

HT = heat treatment; WQ = water quench; AC = air cool; FC = furnace cool over 24 hours

Table 4.2.2. Notched tensile properties of "sensitized" type 316 stainless steel tested at room temperature in air and high-pressure hydrogen and helium gas.

Material	Specimen	Thermal precharging	Test environment	Displacement rate (mm/s)	S_y (MPa)	σ_s (MPa)	RA (%)	Ref.
Rolled rod; HT 1323K, 2h, WQ	(1)	None	Air	8.3 x 10^{-3}	411	723	60	[23]
		None	70 MPa He		429	785	65	
		None	70 MPa H_2		412	778	70	
Rolled rod; HT 1323K, 2h, AC	(1)	None	Air	8.3 x 10^{-3}	374	723	60	[23]
		None	70 MPa He		375	779	65	
		None	70 MPa H_2		387	785	65	
Rolled rod; HT 1323K, 2h, FC	(1)	None	Air	8.3 x 10^{-3}	376	717	60	[23]
		None	70 MPa He		380	790	70	
		None	70 MPa H_2		382	757	70	

HT = heat treatment; WQ = water quench; AC = air cool; FC = furnace cool over 24 hours

(1) V-notched specimen: 60˚ included angle; minimum diameter = 3.4 mm; maximum diameter = 5 mm diameter; maximum root radius = 0.05 mm.

Table 4.3.1. Tensile properties of type 316 stainless steel welds (full penetration, butt joints) tested at room temperature in air and high-pressure hydrogen and helium gas.

Material	Thermal precharging	Test environment	Strain rate (s^{-1})	S_y (MPa)	S_u (MPa)	El_u (%)	El_t (%)	RA (%)	Ref.
EB welded sheet	None	Air	0.6 x10^{-3}	269	562	---	75	70	[23]
	None	70 MPa He		260	574	---	70	70	
	None	70 MPa H_2		256	560	---	75	70	
GTA welded sheet	None	Air	0.6 x10^{-3}	273	572	---	80	70	[23]
	None	70 MPa He		287	585	---	85	70	
	None	70 MPa H_2		272	575	---	85	70	

EB = electron beam; GTA = gas tungsten arc

Table 4.3.2. Notched tensile properties of type 316 stainless steel welds (full penetration, butt joints) tested at room temperature in air and high-pressure hydrogen and helium gas.

Material	Specimen	Thermal precharging	Test environment	displacement rate (mm/s)	S_y (MPa)	σ_s (MPa)	RA (%)	Ref.
EB welded sheet	(1)	None	Air	8.3 x 10^{-3}	393	622	65	[23]
		None	70 MPa He		343	616	65	
		None	70 MPa H_2		351	621	60	
GTA welded sheet	(1)	None	Air	8.3 x 10^{-3}	387	607	65	[23]
		None	70 MPa He		342	614	70	
		None	70 MPa H_2		344	611	65	

EB = electron beam; GTA = gas tungsten arc

(1) Dog-bone notched specimens. Gage: length = 13 mm; width = 5 mm; thickness = 2.3 mm. V-notch centered on the weld bead: 60˚ included angle; depth = 0.6 mm; maximum root radius = 0.05 mm.

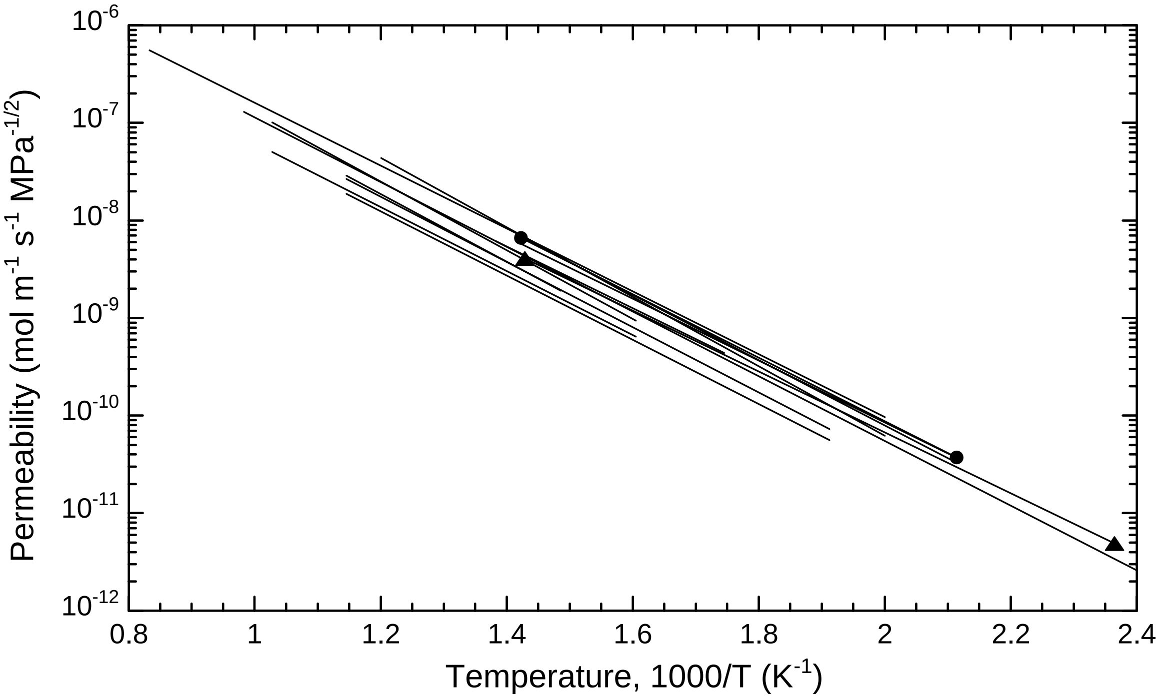

Figure 2.1. Permeability relationships for type 316 stainless steels from a number of references [10, 11, 30-36]. The relationships marked with circles [10] and triangles [11] are averages determined for several austenitic stainless steels, and are given in Table 2.1. Permeability from Ref. [11] is determined for deuterium and has been corrected to give permeability of hydrogen by multiplying by the square root of the mass ratio: $\sqrt{2}$.

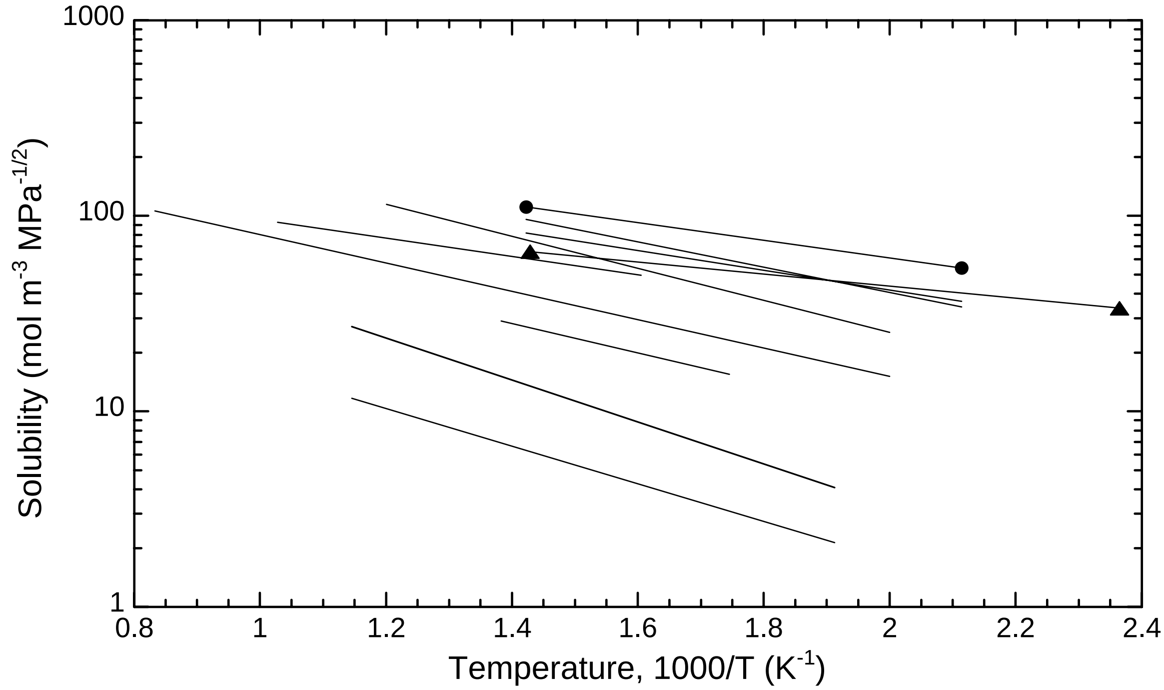

Figure 2.2. Solubility relationships determined from permeability and diffusivity data for type 316 stainless steels from a number of references [10, 11, 30, 32-35]. The relationships marked with circles [10] and triangles [11] are determined from averages for several austenitic stainless steels, and are given in Table 2.1. Data from Ref. [11] are for deuterium.

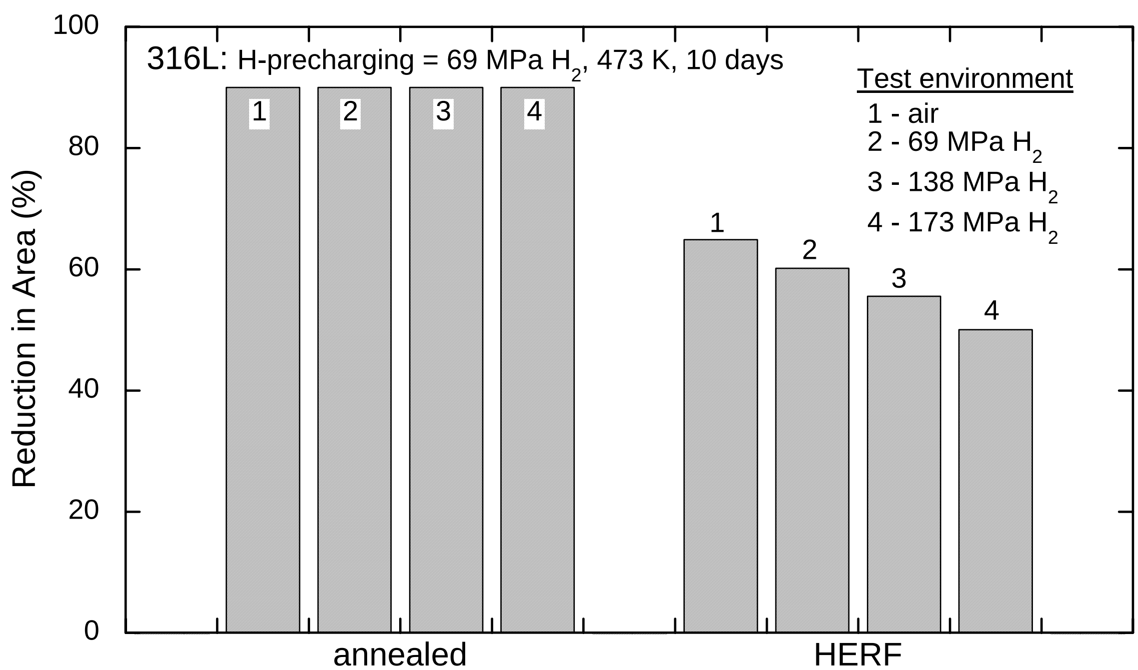

Figure 3.1.1.1. Ductility of smooth tensile specimens of annealed and forged type 316L stainless steel that have been precharged from hydrogen gas at elevated temperature and then tested in hydrogen gas at room temperature. HERF = high energy rate forging [37]

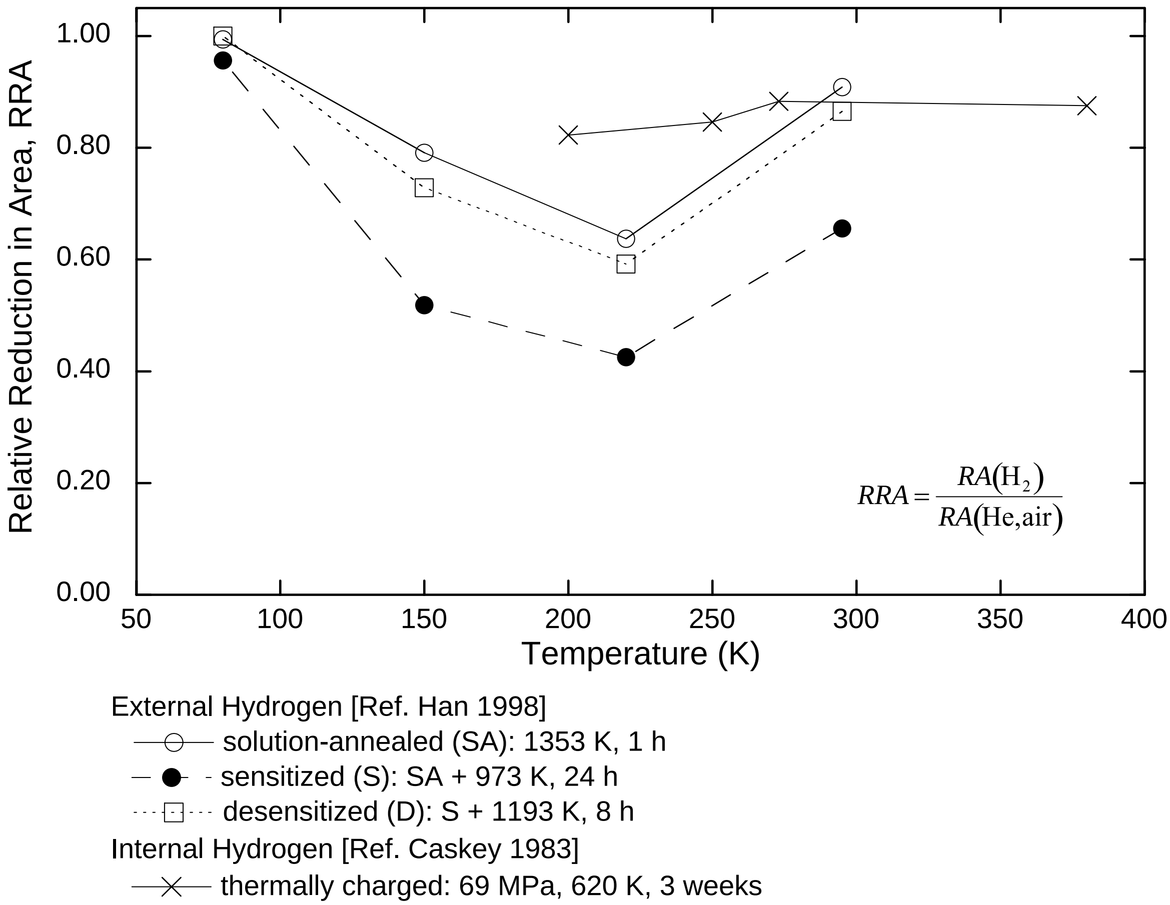

Figure 3.1.1.2. Ductility loss in smooth tensile bars due to hydrogen as a function of temperature, microstructure and hydrogen source. Ref. [5] reports reduction in area in 1 MPa hydrogen gas relative to reduction in area in 1 MPa helium gas at temperatures between 80 and 295 K for annealed and sensitized conditions. Ref. [8] reports reduction in area of thermally precharged specimens tested in air relative to uncharged specimens tested in air between 200 and 380 K (Table 3.1.1.1).

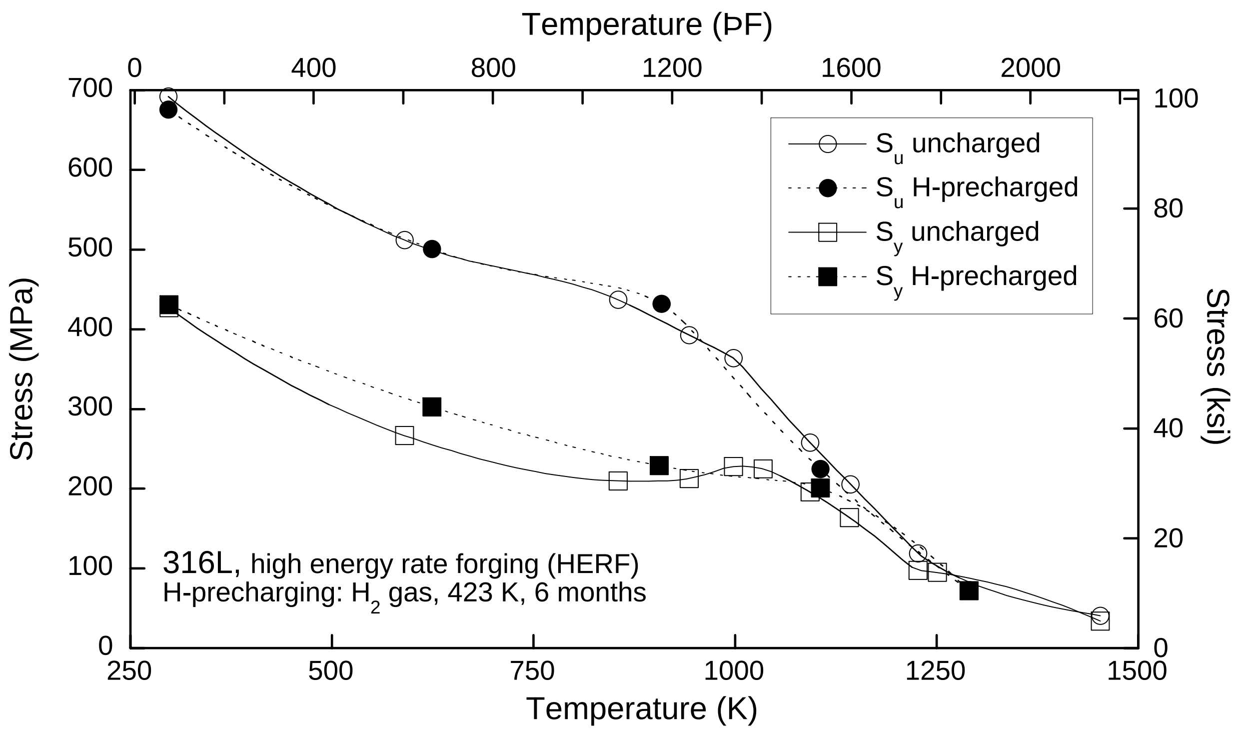

Figure 3.1.1.3. Tensile strength of type 316L stainless steel at elevated temperature in air and thermally precharged in gaseous hydrogen, tested in air. Extension rate = 0.21 mm/s. [17].

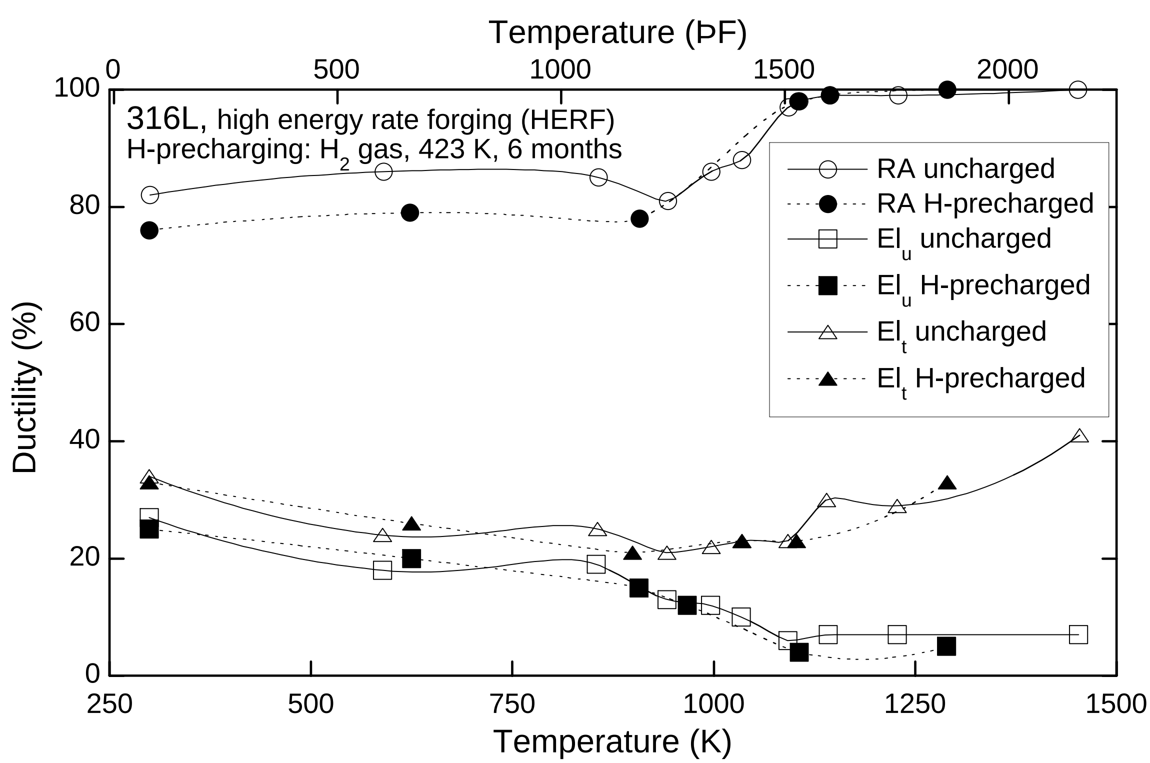

Figure 3.1.1.4. Tensile ductility of type 316L stainless steel at elevated temperature in air and thermally precharged in gaseous hydrogen, tested in air. Extension rate = 0.21 mm/s. [17]